

Full quantum theory for magnon transport in two-sublattice magnetic insulators and magnon junctions

TianYi Zhang¹ and XiuFeng Han^{1,2,3*}

1. *Beijing National Laboratory for Condensed Matter Physics,
Institute of Physics, University of Chinese Academy of Sciences,
Chinese Academy of Sciences, Beijing 100190, China*

2. *Center of Materials Science and Optoelectronics Engineering,
University of Chinese Academy of Sciences, Beijing 100049, China*

3. *Songshan Lake Materials Laboratory, Dongguan, Guangdong 523808, China*

(Dated: April 5, 2023)

Magnon, as elementary excitation in magnetic systems, can carry and transfer angular momentum. Due to the absence of Joule heat during magnon transport, researches on magnon transport have gained considerable interests over the past decade. Recently, a full quantum theory has been employed to investigate magnon transport in ferromagnetic insulators (FMIs). However, the most commonly used magnetic insulating material in experiments, yttrium iron garnet (YIG), is a ferrimagnetic insulator (FIMI). Therefore, a full quantum theory for magnon transport in FIMI needs to be established. Here, we propose a Green's function formalism to compute the magnon bulk and interface current in both FIMIs and antiferromagnetic insulators (AFMIs). We investigate the spatial distribution and temperature dependence of magnon current in FIMIs and AFMIs generated by temperature or spin chemical potential step. In AFMIs, magnon currents generated by temperature step in the two sublattices cancel each other out. Subsequently, we numerically simulate the magnon junction effect using the Green's function formalism, and result shows near 100 % magnon junction ratio. This study demonstrates the potential for investigating magnon transport in specific magnonic devices using a full quantum theory.

Magnon, which is the elementary excitation in magnetic system[1–3], has potential as information carrier due to the ability to carry and transfer angular momentum. Compared to electrons, there are three main advantages of using magnons instead to transport information: Firstly, magnon transport does not generate Joule heat. Xiao et al.'s work shows that magnons can transport in magnetic insulators [4], which avoids the generation of Joule heat. Secondly, magnon is an ideal carrier for transporting GHz or THz information [5–9]. The coherent magnons excited in ferromagnets and antiferromagnets have ranges from GHz to THz eigenfrequency, respectively, which is the spectrum to be developed. Thirdly. There are many ways to inject and detect magnon current. The ways to inject magnons include microwave antenna [10–12], the spin Seebeck effect (SSE) [4, 13–16], and the spin hall effect (SHE) [17]; the detection ways include Brillouin light scattering [18] and the inverse spin hall effect (ISHE) [19, 20]. Recently, there has been an increase in studying spin transport that involves magnons, such as magnon mediate drag effect [21, 22], magnon valve effect [23–25], and magnon junction effect [26]. Like metal-oxide-semiconductor field-effect transistor (MOSFET) in microelectronic devices, magnon junction, composed of a ferromagnetic insulator (FMI1)/antiferromagnetic insulator (AFMI)/ferromagnetic insulator (FMI2), is an elementary device that controls the opening and closing of magnon transport channels. To be more specific, we can

control the magnitude of the output magnon current by manipulating the magnetization state of the two FMI layers. The output magnon current is larger for the parallel state and shorter for the antiparallel state.

In order to further understand the experimental phenomenon, many theories have been proposed for studying magnon transport. For example, the LLG equation, originally introduced by Landau and Lifshitz, and later modified by Gilbert [27] is a classical equation widely used to calculate magnon accumulation and transport [28, 29]. The magnon Schrodinger equation [30–37] is also used to study the wave properties of magnons and their coherent transport. The magnon Boltzmann function [38–41] is used to describe magnon transport from a particle point of view. Recently, Duine et al. propose a Green's function formalism [42, 43] to describe magnon transport in FMIs with and without anisotropy terms. The advantage of this approach is that the Green's function formalism provides a full quantum theory for describing magnon transport, enabling the convenient consideration of disorder and magnon coupling with other particles or quasi-particles. In experiments, one of the most commonly used magnetic materials is yttrium iron garnet (YIG), a ferrimagnetic insulator (FIMI), thus a Green's function formalism for FIMI is needed.

In this paper, we analytically derive the Green's function formalism for magnon transport in FIMI or AFMI. We demonstrate that there are two effective magnon currents in FIMI or AFMI with no interaction between them. And it is reasonable that we could only consider on-site energy and next-nearest neighbor transition energy for these two types of magnons. We also investi-

* xfhan@iphy.ac.cn

gate the spatial distribution of magnon current excited by temperature or spin chemical potential step in FIMI or AFMI, and we calculate the temperature dependence of magnon current, which is consistent with previous research [22]. Furthermore, we study the magnon transport in a magnon junction, simulate the magnon junction effect and the result shows near 100 % magnon junction ratio. Our work demonstrates the possibility of using the Green's function formalism to investigate magnon transport in specific magnonic devices.

The Hamiltonian of FIMI or AFMI, considering the nearest neighbor and next-nearest neighbor Heisenberg exchange interactions, can be expressed as follows:

$$\hat{H} = -J_{AB} \sum_{\langle i,m \rangle} \hat{\mathbf{S}}_i \cdot \hat{\mathbf{S}}_m - J_A \sum_{\langle\langle i,j \rangle\rangle} \hat{\mathbf{S}}_i \cdot \hat{\mathbf{S}}_j - J_B \sum_{\langle\langle m,n \rangle\rangle} \hat{\mathbf{S}}_m \cdot \hat{\mathbf{S}}_n - h_{\text{ext}} \left(\sum_i \mu_A \hat{S}_i^z + \sum_m \mu_B \hat{S}_m^z \right) \quad (1)$$

Where $\langle \rangle$ denotes summing over nearest sites, $\langle\langle \rangle\rangle$ denotes summing over next-nearest sites. J_{AB} and $J_{A(B)}$ represent the nearest and next-nearest Heisenberg exchange interactions strength, respectively. $\mathbf{S}_{i(m)}$ is the spin in A(B) sublattice, $\mu_{A(B)}$ is the magnetic moment in A(B) sublattice. h_{ext} is applied magnetic field along the z direction. Using Holstein-Primakoff (HP) transformation [2], Fourier transformation and Bogoliubov transformation (Details in Supplemental Material [44]) we can get

$$\begin{aligned} \hat{H} &= \sum_k \left[\left[\frac{A_k - B_k}{2} + \frac{\sqrt{(A_k + B_k)^2 - 4C_k^2}}{2} \right] \hat{\alpha}_k^\dagger \hat{\alpha}_k \right. \\ &\quad \left. + \left[\frac{-A_k + B_k}{2} + \frac{\sqrt{(A_k + B_k)^2 - 4C_k^2}}{2} \right] \hat{\beta}_k^\dagger \hat{\beta}_k \right] + \text{const} \quad (2) \\ &\equiv \sum_k (w_k^\alpha \hat{\alpha}_k^\dagger \hat{\alpha}_k + w_k^\beta \hat{\beta}_k^\dagger \hat{\beta}_k) + \text{const} \end{aligned}$$

where $\hat{\alpha}_k$ ($\hat{\beta}_k$), $\hat{\alpha}_k^\dagger$ ($\hat{\beta}_k^\dagger$) are magnon annihilation and creation operators in A(B) sublattice, respectively. $A_k \equiv -2J_A S_A \gamma_{k,nn} - J_{AB} S_B N_n + 2J_A S_A N_{nn} + h_{\text{ext}} \mu_A$, $B_k \equiv -2J_B S_B \gamma_{k,nn} - J_{AB} S_A N_n + 2J_B S_B N_{nn} - h_{\text{ext}} \mu_B$, $C_k \equiv -J_{AB} \sqrt{S_A S_B} \gamma_{k,n}$, N_n , N_{nn} are the numbers of nearest and the next-nearest sites, respectively. In the case of one-dimensional atomic chain model, $N_n = N_{nn} = 2$, $\gamma_{k,n} = 2\cos(ka)$, $\gamma_{k,nn} = 2\cos(2ka)$, where a is the distance between nearest sites. Thus, in both FIMI or AFMI, the magnon currents can be separated into two uncoupled magnon currents with opposite polarity. Specifically, in AFMI, $J_A = J_B$, $S_A = S_B$, $\mu_A = \mu_B$, but in FIMI, the above equation does not hold.

Eq. (2) shows that in FIMI or AFMI, considering the nearest neighbor and next-nearest neighbor Heisenberg exchange interactions, it can still be thought there are two independent types of magnons in it. We can use Fourier transformation to Eq. (2) to transform Hamiltonian of FIMI or AFMI to coordinate space, and get

$$w_k^{\alpha(\beta)} = \sum_{n=0}^{\infty} 2A_n(B_n) \cos(nka) \quad (3)$$

Where A_0 (B_0) and A_1 (B_1) represent on-site and nearest transition energy of magnons in A (B) sublattice. Then the Hamiltonian can be written as

$$\hat{H} = \sum_{n=0}^{\infty} \sum_{i,j} \delta(i-j \pm n) \left(A_n \alpha_i^\dagger \alpha_j + B_n \beta_i^\dagger \beta_j \right) \quad (4)$$

From Eq. (2~4), we can see that for one-dimensional atomic chain model $A_{2n+1} = B_{2n+1} = 0$ ($n = 0, 1, 2 \dots$), which means that magnons can only propagate between sites that are an even number of lattice constants away from each other. We investigate the variation of the Fourier expansion coefficient with expansion order, where for AFMI we use the following parameters [45, 46]: $J_{AB} = -0.002$ eV, $J_A = J_B = 0.02$ eV, $S_A = S_B = 1$, and for FIMI we use the following plausible parameters [29]: $J_{AB} = -0.005$ eV, $J_A = 0.05$ eV, $J_B = 0.01$ eV, $S_A = 1$, $S_B = 1.5$, as shown in Fig. 1. We can see that for both AFMI and FIMI the odd parts of the expansion coefficients are consistently 0, while the even parts approach 0 when $n > 4$, indicating that only two terms A_0 (B_0) and A_2 (B_2) need to be retained.

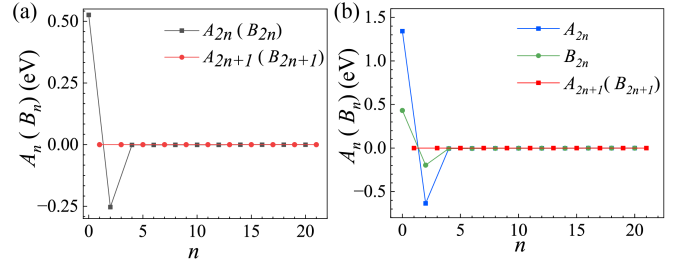


FIG. 1. The variation of the Fourier expansion coefficient with expansion order n for AFMI (a) and FIMI (b).

Then we study the magnon transport in FIMI or AFMI, only two terms A_0 (B_0) and A_2 (B_2) are taken into account. A schematic diagram that illustrates the transport of magnon current through FIMI or AFMI is shown in Fig. 2. In this setup, the FIMI or AFMI is connected to two heavy metals (HMs) with temperatures T_R , T_L and spin chemical potentials μ_L , μ_R , respectively. The magnon current is driven by the difference of temperature or spin chemical potential between two HMs. To calculate the bulk magnon current, we need to calculate the retarded and advanced Green's functions firstly. This can be accomplished by using the Dyson equation

$$\mathcal{G}^{R(A)}(\varepsilon) = \left[\varepsilon^{+(-)} - H - \hbar \Sigma^{R(A)}(\varepsilon) \right]^{-1} \quad (5)$$

Where $\mathcal{G}^{R(A)}$ is retarded (advanced) Green's function, $\varepsilon^{+(-)} = \varepsilon + (-)i\eta$, η is a infinitesimal positive number, H is Hamiltonian of magnons in FIMI or AFMI, and $\Sigma^{R(A)}(\varepsilon)$ is retarded (advanced) self-energy, which describes the coupling between FIMI or AFMI and external system. For FIMI or AFMI, the Hamiltonian is



FIG. 2. Schematic diagram that illustrates the transport of magnon current through FIMI or AFMI driven by temperature or spin chemical potential difference.

$$\hat{H} = \sum_{i,j} [(A_0 \delta_{i,j} + A_2 \delta_{i,j\pm 2}) \hat{\alpha}_i^\dagger \hat{\alpha}_j + (B_0 \delta_{i,j} + B_2 \delta_{i,j\pm 2}) \hat{\beta}_i^\dagger \hat{\beta}_j] \quad (6)$$

and the self-energy are composed of three items $\Sigma^{R(A)}(\varepsilon) = \Sigma_C^{R(A)}(\varepsilon) + \sum_{r \in \{L,R\}} \Sigma_r^{R(A)}(\varepsilon)$, where

$$\Sigma_C^{R(A)}(\varepsilon) = \mp i \alpha (\varepsilon - \mu_C) \delta_{i,j} / \hbar,$$

$$\Sigma_L^{R(A)} = \mp i \eta^L (\varepsilon - \mu_L) \delta_{i,j} (\delta_{j,1} + \delta_{j,2}) / \hbar$$

$$\Sigma_R^{R(A)} = \mp i \eta^R (\varepsilon - \mu_R) \delta_{i,j} (\delta_{j,N} + \delta_{j,N-1}) / \hbar \quad (7)$$

are retarded (advanced) self-energy induced by Gilbert damping in FIMI or AFMI, connection with left HM and right HM, respectively. Where α is Gilbert damping in FIMI or AFMI, \hbar is reduced Planck's constant, $\eta^{L(R)}$ is parameter that shows the coupling with left and right HMs [43, 47], $\mu_{L(R)}$ is spin chemical potential of left(right) HM, μ_C is magnon potential of FIMI or AFMI.

Secondly, we can calculate the magnon density matrix using langreth rule [43]

$$\rho = \int_{-\infty}^{\infty} \frac{d\varepsilon}{2\pi} [\mathcal{G}^R(\varepsilon) i \hbar \Sigma^<(\varepsilon) \mathcal{G}^A(\varepsilon)] \quad (8)$$

where the less self-energy can be calculated by

$$\begin{aligned} \Sigma^<(\varepsilon) &= \Sigma_C^<(\varepsilon) + \sum_{r \in \{L,R\}} \Sigma_r^<(\varepsilon) \\ &= 2i N_B \left(\frac{\varepsilon - \mu_C}{k_B T_C} \right) \text{Im}(\Sigma_C^R(\varepsilon)) \\ &\quad + \sum_{r \in \{L,R\}} 2i N_B \left(\frac{\varepsilon - \mu_r}{k_B T_r} \right) \text{Im}(\Sigma_r^R(\varepsilon)) \end{aligned} \quad (9)$$

Where $N_B(x) = \frac{1}{e^x - 1}$ is Bose-Einstein distribution. Then we can calculate bulk magnon current using Heisenberg motion equation.

$$\hbar \frac{d \langle \alpha_i^\dagger \alpha_i \rangle}{dt} = \sum_j -i (h_{i,j} \rho_{j,i} - h_{j,i} \rho_{i,j}) = \sum_j j_{m,i,j} \quad (10)$$

where $j_{m,i,j}$ represents the magnon current from site i to site j , h is Hamiltonian for α mode magnons. Eq. (10) indicates that the change in the magnon number at site i is caused by all magnon currents from site i to other sites.

According to [22], the magnetization reversal of the ferromagnetic (FM) layer has no effect on the transport of magnon current induced by the spin Hall effect (SHE). However, for magnon current induced by the spin Seebeck effect (SSE), the opposite magnetization of the FM generates magnons of different signs, leading to a output voltage signal with opposite signs. Therefore, we assume that magnons with opposite polarity experience an equivalent spin voltage but an opposite temperature gradient.

The Green's function formalism can also be utilized to calculate the interface magnon current. By using the Landauer-Büttiker formula [43], we find that the magnon current at the interface between FIMI or AFMI and HMs can be expressed as follows:

$$\begin{aligned} j_{L(R)}^m &= j_{L(R),\alpha}^m + j_{L(R),\beta}^m \\ &= \int \frac{d\varepsilon}{2\pi} \left[N_B \left(\frac{\varepsilon - \mu_{L(R)}}{k_B T_{L(R)}} \right) - N_B \left(\frac{\varepsilon - \mu_{R(L)}}{k_B T_{R(L)}} \right) \right] T_{b,\alpha}(\varepsilon) \\ &\quad + \int \frac{d\varepsilon}{2\pi} \left[N_B \left(\frac{\varepsilon - \mu_{L(R)}}{k_B T_{L(R)}} \right) - N_B \left(\frac{\varepsilon - \mu_C}{k_B T_{AFMI}} \right) \right] T_{f,\alpha}(\varepsilon) \\ &\quad + \int \frac{d\varepsilon}{2\pi} \left[N_B \left(\frac{\varepsilon - \mu_{L(R)}}{k_B T_{L(R)}} \right) - N_B \left(\frac{\varepsilon - \mu_{R(L)}}{k_B T_{L(R)}} \right) \right] T_{b,\beta}(\varepsilon) \\ &\quad + \int \frac{d\varepsilon}{2\pi} \left[N_B \left(\frac{\varepsilon - \mu_{L(R)}}{k_B T_{AFMI}} \right) - N_B \left(\frac{\varepsilon - \mu_C}{k_B T_{L(R)}} \right) \right] T_{f,\beta}(\varepsilon) \end{aligned} \quad (11)$$

Where the transmission function

$$\begin{aligned} T_{b,i}(\varepsilon) &\equiv \text{Tr} \left[\hbar \Gamma_{L(R),i}^R(\varepsilon) \mathcal{G}_i^R(\varepsilon) \hbar \Gamma_{R(L),i}(\varepsilon) \mathcal{G}_i^A(\varepsilon) \right], \\ T_{f,i}(\varepsilon) &\equiv \text{Tr} \left[\hbar \Gamma_{L(R),i}^R(\varepsilon) \mathcal{G}_i^R(\varepsilon) \hbar \Gamma_{AFMI}(\varepsilon) \mathcal{G}_i^A(\varepsilon) \right] \end{aligned} \quad (12)$$

Where $i = \alpha$ or β , are two modes of magnons with opposite polarity, the rates $\Gamma_{L(R),i}(\varepsilon) = -2\text{Im}(\Sigma_{L(R),i}^R(\varepsilon))$.

The Green's function formalism can be utilized to calculate magnon current driven by different driving mechanisms, such as temperature difference or spin chemical potential difference. In particular, we use temperature difference between left and right HMs to simulate magnon current excited by SSE, and use spin chemical difference between left and right HMs to simulate magnon current excited by SHE. And we use a one-dimensional atomic chain model for simplicity.

To investigate the spatial distribution and temperature dependence of magnon currents in AFMI excited by the SSE and the SHE, we set the temperature difference (ΔT) and spin chemical potential difference ($\Delta \mu$) between two HMs. The corresponding results are shown in Fig. 3. In Fig. 3. (a), we calculated spatial distribution of magnon currents excited by SSE in AFMI. The parameters used in simulation are set to be $A_0 = B_0 = 0.5$ eV, $A_2 = B_2 = -0.25$ eV, total site number $N = 100$, applied magnetic field $h_{ext} = 0$, spin chemical potential $\mu_L = \mu_R = 0$, $\eta^L = \eta^R = 8$, temperature $k_B T_{AFMI} = 0.26$ eV, $T_L = 1.2 T_{AFMI}$, $T_R = 0.8 T_{AFMI}$, magnon potential $\mu_{AFMI} = 0$ and Gilbert damping $\alpha_{AFMI} = 0.001$ [48].

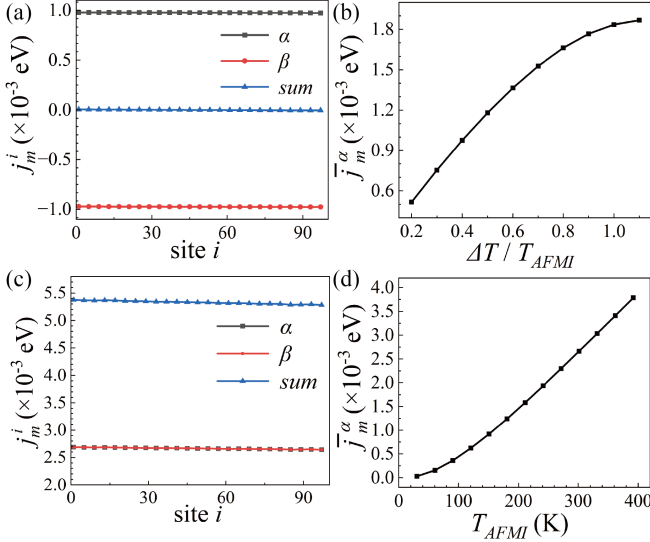


FIG. 3. Spatial distribution and temperature dependence of magnon currents excited by SSE (a, b) and SHE (c, d) in AFMI.

We can see that the magnon currents composed of α and β modes magnons have different sign but the same absolute value, so the α and β mode magnon currents cancel with each other, total magnon current j_m^{sum} is 0. Then we keep the temperature of left HM $T_L = 1.2 T_{AFMI}$ fixed, change the temperature of right HM T_R , and average all the α mode magnon current of 100 sites, the temperature dependence of averaged α mode magnon currents \bar{j}_m^α is shown in Fig. 3. (b), we can see that \bar{j}_m^α shows positive correlation dependence on temperature difference between left and right HMs $\Delta T = T_L - T_R$ and the influence of ΔT on \bar{j}_m^α is gradually reduced as ΔT increases. Then we calculated spatial distribution of magnon currents excited by SHE in AFMI, see Fig. 3. (c). Spin chemical potential $\mu_L = 0.1A_0$, $\mu_R = 0$, temperature $k_B T_{AFMI} = 0.026$ eV, $T_L = T_R = T_{AFMI}$. We can see that for magnon current excited by SHE, α and β mode magnons contribute equally in the component of sum magnon currents. And then we change the temperature of left HM, AFMI and right HM at the same time, and calculate the temperature dependence of average α mode magnon current, as shown in Fig. 3. (d). We can see that \bar{j}_m^α increases as T_{AFMI} increases. It can be explained by that as T_{AFMI} increase, the number of α mode magnon in sublattice $n_\alpha(\varepsilon) = \frac{1}{e^{k_B T_{AFMI} \varepsilon} - 1}$ increases, therefore, the magnons involved in transport increase.

Then we calculate the spatial distribution and temperature dependence of magnon currents in FIMI excited by the SSE and the SHE, as shown in Fig. 4. In Fig. 4. (a), we calculated spatial distribution of magnon currents excited by SSE in FIMI. The parameters used in simulation are set to be $A_0 = 1.3$ eV, $B_0 = 0.43$ eV, $A_2 = -0.6$ eV, $B_2 = -0.2$ eV, site number $N = 100$, ap-

plied magnetic field $h_{ext} = 0$, spin chemical potential $\mu_L = \mu_R = 0$, $\eta^L = \eta^R = 8$, temperature $k_B T_{AFMI} = 0.026$ eV, $T_L = 1.2 T_{AFMI}$, $T_R = 0.8 T_{AFMI}$, magnon potential $\mu_{FIMI} = 0$ and Gilbert damping $\alpha_{FIMI} = 0.001$. We can see that although magnon currents generated by α and β mode magnons have opposite sign, they do not cancel with each other, which means sum magnon current j_m^{sum} is not equal to 0 in FIMI. Then we keep left HM temperature $T_L = 1.2 T_{AFMI}$ fixed, change the right HM temperature T_R , calculate the site average magnon current \bar{j}_m^α , \bar{j}_m^β , \bar{j}_m^{sum} dependence on the temperature difference, see Fig. 4. (b) we can see the absolute value of \bar{j}_m^α , \bar{j}_m^β , \bar{j}_m^{sum} increase as temperature difference between left and right HMs ΔT increases. As for magnon current excited by SHE in FIMI, we set parameters to be spin chemical potential $\mu_L = 0.1A_0$, $\mu_R = 0$, temperature $k_B T_{AFMI} = 0.026$ eV, $T_L = T_R = T_{AFMI}$, and calculate the space distribution of magnon current. We can see from Fig. 4. (c) that in FIMI due to the difference of on-site and next-nearest transition energy between α and β mode magnons, the magnon currents composed by these two types of magnons are not the same. And then we change the temperature of the whole system at the same time, and calculate the temperature dependence of average magnon current \bar{j}_m^α , \bar{j}_m^β , \bar{j}_m^{sum} . We can see from Fig. 4. (d) that \bar{j}_m^α , \bar{j}_m^β , \bar{j}_m^{sum} all increase as system temperature increase, which is due to the increase of magnons in two sublattices.

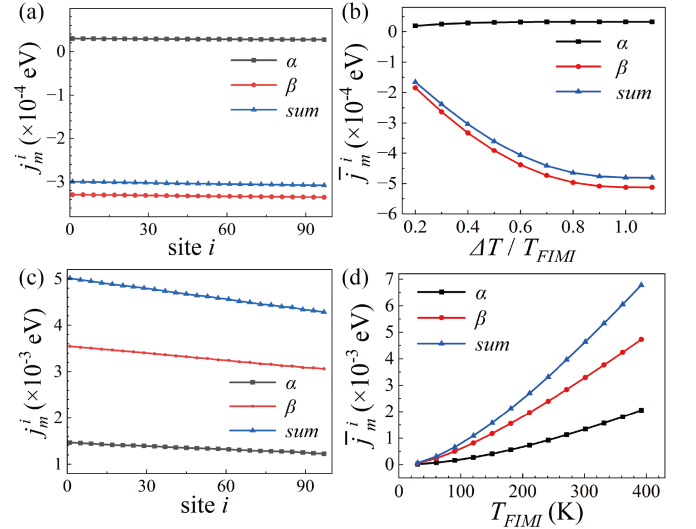


FIG. 4. Spatial distribution and temperature dependence of magnon currents excited by SSE (a, b) and SHE (c, d) in FIMI.

Magnon junction is a magnon-conductive device that consists of an FMI1/AFMI/FMI2 structure with a high on-off ratio between parallel and antiparallel state of two FMI layers. We can use Green's function formalism to simulate magnon junction effect. The model includes a magnon junction and two HM leads, as shown in Fig.

5. By fixing the magnetization of FMI1 in the upward direction and varying the magnetization of FMI2 between up and down state, we can set the magnon junction to be parallel or antiparallel state. The Hamiltonian of the

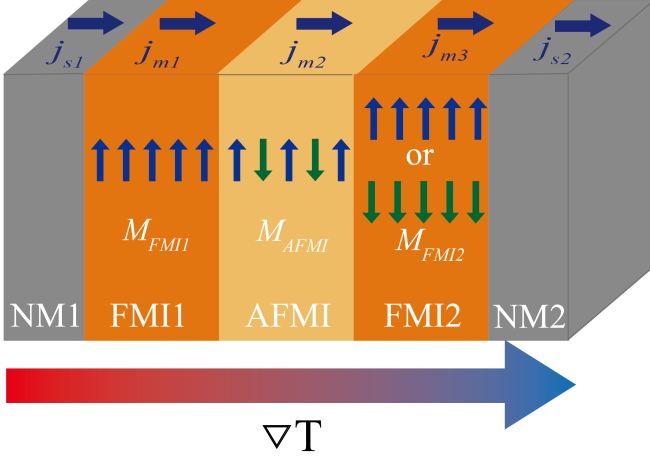


FIG. 5. Schematic diagram of magnon current driven by temperature gradient transporting through a magnon junction.

magnon junction is composed of five items

$$\hat{H} = \hat{H}_{FMI1} + \hat{H}_{AFMI} + \hat{H}_{FMI2} + \hat{H}_{FMI1,AFMI} + \hat{H}_{FMI2,AFMI} \quad (13)$$

Where \hat{H}_{FMI1} , \hat{H}_{AFMI} , \hat{H}_{FMI2} are Hamiltonian of FMI1, AFMI and FMI2, respectively, and $\hat{H}_{FMI1,AFMI}$, $\hat{H}_{FMI2,AFMI}$ are coupling between FMI1 and AFMI, FMI2 and AFMI, respectively. Only on-site and next-nearest transition energy are considered. For parallel state:

$$\hat{H}_{FMI1(2)} = \sum_{i,j} [(A_0^{FMI1(2)} \delta_{i,j} + A_2^{FMI1(2)} \delta_{i,j\pm 2}) \hat{\alpha}_i^\dagger \hat{\alpha}_j] \quad (14)$$

$$\hat{H}_{AFMI} = \sum_{i,j} [(A_0^{AFMI} \delta_{i,j} + A_2^{AFMI} \delta_{i,j\pm 2}) \hat{\alpha}_i^\dagger \hat{\alpha}_j + (B_0^{AFMI} \delta_{i,j} + B_2^{AFMI} \delta_{i,j\pm 2}) \hat{\beta}_i^\dagger \hat{\beta}_j] \quad (15)$$

$$\hat{H}_{FMI1(2),AFMI} = J_{FMI1(2),AFMI} (\hat{\alpha}_{end(1),FMI1(2)}^\dagger \hat{\alpha}_{1(end),AFMI} + \hat{\alpha}_{end(1),FMI1(2)}^\dagger \hat{\beta}_{1(end),AFMI}) + H.c. \quad (16)$$

, and for antiparallel state, all the $\hat{\alpha}$ ($\hat{\alpha}^\dagger$) in Hamiltonian of \hat{H}_{FMI2} and $\hat{\alpha}_{FMI2}$ ($\hat{\alpha}_{FMI2}^\dagger$) in Hamiltonian of $\hat{H}_{FMI2,AFMI}$ are replaced by $\hat{\beta}$ ($\hat{\beta}^\dagger$) and $\hat{\beta}_{FMI2}$ ($\hat{\beta}_{FMI2}^\dagger$).

We can use Eqs. (11~16) to calculate magnon currents in three parts of magnon junction. The boundary conditions are set to be that magnon currents are continuous at interface and there are no magnon current injected from NM1 to FMI1. The simulation parameters are set to be on-site energy $A_0^{FMI1} = A_0^{FMI2} = A_0^{AFMI} = B_0^{AFMI} = 0.5$ eV, nearest transition energy $A_1^{FMI1} = A_1^{FMI2} = -0.5$ eV, $A_1^{AFMI} = B_1^{AFMI} = -0.25$ eV, coupling energy of two types of magnons $J_{FMI1,AFMI} = J_{FMI2,AFMI} = 1$ eV, spin chemical potential of two HMs layer $\mu_{NM1} = \mu_{NM2} = 0$, temperature $k_B T_{NM1} = 0.026$ eV, $T_{FMI1} = 0.9 T_{NM1}$, $T_{AFMI} = 0.8 T_{NM1}$, $T_{FMI2} = 0.7 T_{NM1}$, $T_{NM2} = 0.6 T_{NM1}$, total site number $N_{FMI1} = N_{AFMI} = N_{FMI2} = 20$, coupling with two HMs layers $\eta^{L(R)} = 8$ and Gilbert damping constant $\alpha_{FMI1} = \alpha_{FMI2} = 0.01$, $\alpha_{AFMI} = 0.001$ (Details of different part's self-energy are in Supplemental Material [44]). Boundary condition is a nonlinear system of first order equations, and we can get a rough solution of μ_{FMI1} , μ_{AFMI} , μ_{FMI2} .

For parallel magnetization, magnon potentials are $\mu_{FMI1} = 20$ meV, $\mu_{AFMI} = 5.3$ meV, $\mu_{FMI2} = 18$ meV, and the magnon current at the interface of FMI2 and HM2 is 6.53×10^{-4} eV; for antiparallel magnetization state, magnon potentials are $\mu_{FMI1} = -37$ meV, $\mu_{AFMI} = 5.2$ meV, $\mu_{FMI2} = -36.8$ meV, and the magnon current at the interface of FMI2 and HM2 is 4.79×10^{-7} eV. It shows near 100 % magnon junction ratio, here magnon junction ratio is $MJR = (J_{m,\uparrow\uparrow} - J_{m,\uparrow\downarrow}) / (J_{m,\uparrow\uparrow} + J_{m,\uparrow\downarrow})$, where $J_{m,\uparrow\uparrow}$ and $J_{m,\uparrow\downarrow}$ are output magnon current of parallel magnetization and antiparallel magnetization state.

In conclusion, we propose a Green's function formalism to investigate magnon transport in AFMI or FIMI, which is a full quantum theory to study magnon transport in two-sublattice magnetic insulators. We studied the spatial distribution and temperature dependence of magnon current generated by the temperature or spin chemical potential step in FIMI or AFMI. Our results reveal that the magnon currents in both sublattices exhibit a positive correlation with temperature, and in AFMI, the magnon currents generated by temperature step in the two sublattices cancel each other out. Furthermore, we numerically simulate the magnon junction effect using the Green's function formalism, which yields a near 100 % magnon junction ratio. Our work demonstrates the potential of employing full quantum theory to study magnon transport in specific magnonic devices.

This work is financial supported by the National Key Research and Development Program of China (MOST) (Grant No. 2022YFA1402800), the National Natural Science Foundation of China (NSFC) (Grant No. 51831012, 12134017), and partially supported by the Strategic Priority Research Program (B) (Grant No. XDB33000000).

-
- [1] A. V. Chumak, V. Vasyuchka, A. Serga, and B. Hillebrands, Magnon spintronics, *Nature Physics* **11**, 453 (2015).
- [2] H. Y. Yuan, Y. Cao, A. Kamra, R. A. Duine, and P. Yan, Quantum magnonics: When magnon spintronics meets quantum information science, *Physics Reports* **965**, 1 (2022).
- [3] F. Bloch, Zur theorie des ferromagnetismus, *Zeitschrift für Physik* **61**, 206 (1930).
- [4] J. Xiao, G. E. W. Bauer, K.-c. Uchida, E. Saitoh, and S. Maekawa, Theory of magnon-driven spin seebeck effect, *Physical Review B* **81**, 214418 (2010).
- [5] J. D. Adam, Analog signal processing with microwave magnetics, *Proceedings of the IEEE* **76**, 159 (1988).
- [6] V. Cherepanov, I. Kolokolov, and V. L'Vov, The saga of yig: Spectra, thermodynamics, interaction and relaxation of magnons in a complex magnet, *Physics Reports* **229**, 81 (1993).
- [7] J. M. Owens, J. H. Collins, and R. L. Carter, System applications of magnetostatic wave devices, *Circuits Systems and Signal Processing* **4**, 317 (1985).
- [8] T. Balashov, P. Buczek, L. Sandratskii, A. Ernst, and W. Wulfhekel, Magnon dispersion in thin magnetic films, *J Phys Condens Matter* **26**, 394007 (2014).
- [9] T. H. Chuang, K. Zakeri, A. Ernst, Y. Zhang, H. J. Qin, Y. Meng, Y. J. Chen, and J. Kirschner, Magnetic properties and magnon excitations in fe(001) films grown on ir(001), *Phys.rev.b* **89**, 1493 (2014).
- [10] T. Schneider, A. A. Serga, T. Neumann, B. Hillebrands, and M. P. Kostylev, Phase reciprocity of spin-wave excitation by a microstrip antenna, *Physical Review B* **77**, 214411 (2008).
- [11] M. Jamali, J. H. Kwon, S. M. Seo, K. J. Lee, and H. Yang, Spin wave nonreciprocity for logic device applications, *Sci Rep* **3**, 3160 (2013).
- [12] Vladislav, E., Demidov, Mikhail, P., Kostylev, Karsten, Rott, Patryk, and Krzysteczko, Excitation of microwaveguide modes by a stripe antenna, *Applied Physics Letters* **95**, 257202 (2009).
- [13] J.-i. Ohe, H. Adachi, S. Takahashi, and S. Maekawa, Numerical study on the spin seebeck effect, *Physical Review B* **83**, 115118 (2011).
- [14] G. E. W. Bauer, E. Saitoh, and B. J. van Wees, Spin caloritronics, *Nature Materials* **11**, 391 (2012).
- [15] H. Yu, S. D. Brechet, and J.-P. Ansermet, Spin caloritronics, origin and outlook, *Physics Letters A* **381**, 825 (2017).
- [16] S. M. Rezende, R. Rodriguez-Surez, R. O. Cunha, A. R. Rodrigues, F. Machado, G. Guerra, J. Ortiz, and A. Azevedo, Magnon spin-current theory for the longitudinal spin-seebeck effect, *Physical Review B* (2014).
- [17] J. Sinova, S. O. Valenzuela, J. Wunderlich, C. Back, and T. Jungwirth, Spin hall effects, *Reviews of Modern Physics* **87**, 1213 (2015).
- [18] S. O. Demokritov, B. Hillebrands, and A. N. Slavin, Brillouin light scattering studies of confined spin waves: linear and nonlinear confinement, *Physics Reports* **348**, 441 (2001).
- [19] L. K. Werake, B. A. Ruzicka, and H. Zhao, Observation of intrinsic inverse spin hall effect, *Physical Review Letters* **106**, 107205 (2011).
- [20] Saitoh, E., Ueda, M., Miyajima, H., Tatara, and G., Conversion of spin current into charge current at room temperature: Inverse spin-hall effect, *Applied Physics Letters* **88**, 182509 (2006).
- [21] S. S. Zhang and S. Zhang, Magnon mediated electric current drag across a ferromagnetic insulator layer, *Phys Rev Lett* **109**, 096603 (2012).
- [22] H. Wu, C. H. Wan, X. Zhang, Z. H. Yuan, Q. T. Zhang, J. Y. Qin, H. X. Wei, X. F. Han, and S. Zhang, Observation of magnon-mediated electric current drag at room temperature, *Physical Review B* **93**, 10.1103/PhysRevB.93.060403 (2016).
- [23] H. Wu, L. Huang, C. Fang, B. S. Yang, C. H. Wan, G. Q. Yu, J. F. Feng, H. X. Wei, and X. F. Han, Magnon valve effect between two magnetic insulators, *Phys Rev Lett* **120**, 097205 (2018).
- [24] L. Cornelissen, J. Liu, B. van Wees, and R. Duine, Spin-current-controlled modulation of the magnon spin conductance in a three-terminal magnon transistor, *Physical Review Letters* **120**, 097702 (2018).
- [25] J. Cramer, F. Fuhrmann, U. Ritzmann, V. Gall, T. Nizeki, R. Ramos, Z. Qiu, D. Hou, T. Kikkawa, J. Sinova, U. Nowak, E. Saitoh, and M. Klui, Magnon detection using a ferroic collinear multilayer spin valve, *Nature Communications* **9**, 1089 (2018).
- [26] C. Y. Guo, C. H. Wan, X. Wang, C. Fang, P. Tang, W. J. Kong, M. K. Zhao, L. N. Jiang, B. S. Tao, G. Q. Yu, and X. F. Han, Magnon valves based on yig/nio/yig all-insulating magnon junctions, *Physical Review B* **98**, 10.1103/PhysRevB.98.134426 (2018).
- [27] T. L. Gilbert, Classics in magnetics a phenomenological theory of damping in ferromagnetic materials, *IEEE Transactions on Magnetism* **40**, 3443 (2004).
- [28] U. Ritzmann, D. Hinzke, and U. Nowak, Propagation of thermally induced magnonic spin currents, *Physical Review B* **89**, 10.1103/PhysRevB.89.024409 (2014).
- [29] U. Ritzmann, D. Hinzke, and U. Nowak, Thermally induced magnon accumulation in two-sublattice magnets, *Physical Review B* **95**, 10.1103/PhysRevB.95.054411 (2017).
- [30] P. Yan, X. S. Wang, and X. R. Wang, All-magnonic spin-transfer torque and domain wall propagation, *Phys. Rev. Lett.* **107**, 177207 (2011).
- [31] W. Wang, M. Albert, M. Beg, M.-A. Bisotti, D. Chernyshenko, D. Cortés-Ortuño, I. Hawke, and H. Fangohr, Magnon-driven domain-wall motion with the dzyaloshinskii-moriya interaction, *Phys. Rev. Lett.* **114**, 087203 (2015).
- [32] J. Lan, W. Yu, R. Wu, and J. Xiao, Spin-wave diode, *Phys. Rev. X* **5**, 041049 (2015).
- [33] C. Jia, D. Ma, A. F. Schffer, and J. Berakdar, Twisted magnon beams carrying orbital angular momentum, *Nature Communications* **10**, 2077 (2019).
- [34] W. Yu, J. Lan, R. Wu, and J. Xiao, Magnetic snell's law and spin-wave fiber with dzyaloshinskii-moriya interaction, *Phys. Rev. B* **94**, 140410 (2016).
- [35] Y. W. Xing, Z. R. Yan, and X. F. Han, Magnon valve effect and resonant transmission in a one-dimensional magnonic crystal, *Phys. Rev. B* **103**, 054425 (2021).
- [36] Z. Wang, Y. Cao, and P. Yan, Goos-hänchen effect of spin waves at heterochiral interfaces, *Phys. Rev. B* **100**,

- 064421 (2019).
- [37] S.-J. Lee, J.-H. Moon, H.-W. Lee, and K.-J. Lee, Spin-wave propagation in the presence of inhomogeneous dzyaloshinskii-moriya interactions, *Phys. Rev. B* **96**, 184433 (2017).
- [38] A. Manchon and S. Zhang, Theory of nonequilibrium intrinsic spin torque in a single nanomagnet, *Physical Review B* **78**, 10.1103/PhysRevB.78.212405 (2008).
- [39] L. J. Cornelissen, K. J. H. Peters, G. E. W. Bauer, R. A. Duine, and B. J. van Wees, Magnon spin transport driven by the magnon chemical potential in a magnetic insulator, *Physical Review B* **94**, 10.1103/PhysRevB.94.014412 (2016).
- [40] T. Liu, W. Wang, and J. Zhang, Collective induced antidiffusion effect and general magnon boltzmann transport theory, *Physical Review B* **99**, 10.1103/PhysRevB.99.214407 (2019).
- [41] J. Sinova, D. Culcer, Q. Niu, N. A. Sinitsyn, T. Jungwirth, and A. H. MacDonald, Universal intrinsic spin hall effect, *Phys Rev Lett* **92**, 126603 (2004).
- [42] W. P. Sterk, H. Y. Yuan, A. Rckriegel, B. Z. Rameshti, and R. A. Duine, Green's function formalism for nonlocal elliptical magnon transport, *Physical Review B* **104**, 10.1103/PhysRevB.104.174404 (2021).
- [43] J. Zheng, S. Bender, J. Armaitis, R. E. Troncoso, and R. A. Duine, Green's function formalism for spin transport in metal-insulator-metal heterostructures, *Physical Review B* **96**, 10.1103/PhysRevB.96.174422 (2017).
- [44] See supplemental material at supplemental material, which includes a explicit calculations of the hamiltonian of fimi or afmi and the self-energy., .
- [45] D. Ködderitzsch, W. Hergert, W. M. Temmerman, Z. Szotek, A. Ernst, and H. Winter, Exchange interactions in nio and at the nio(100) surface, *Phys. Rev. B* **66**, 064434 (2002).
- [46] W.-B. Zhang, Y.-L. Hu, K.-L. Han, and B.-Y. Tang, Pressure dependence of exchange interactions in NiO, *Phys. Rev. B* **74**, 054421 (2006).
- [47] Y. Tserkovnyak, A. Brataas, and G. E. Bauer, Enhanced gilbert damping in thin ferromagnetic films, *Phys Rev Lett* **88**, 117601 (2002).
- [48] T. Moriyama, K. Hayashi, K. Yamada, M. Shima, Y. Ohya, and T. Ono, Intrinsic and extrinsic antiferromagnetic damping in nio, *Phys. Rev. Mater.* **3**, 051402 (2019).
- [49] V. Baltz, A. Manchon, M. Tsoi, T. Moriyama, T. Ono, and Y. Tserkovnyak, Antiferromagnetic spintronics, *Reviews of Modern Physics* **90**, 015005 (2018).
- [50] M. V. Costache, M. Sladkov, S. M. Watts, C. Wal, and B. Wees, Electrical detection of spin pumping due to the precessing magnetization of a single ferromagnet, *Physical Review Letters* **97**, 216603 (2006).
- [51] K.-S. Lee, S.-W. Lee, B.-C. Min, and K.-J. Lee, Threshold current for switching of a perpendicular magnetic layer induced by spin hall effect, *Applied Physics Letters* **102**, 10.1063/1.4798288 (2013).
- [52] Y. W. Xing, Z. R. Yan, and X. F. Han, Comparison of spin-wave transmission in parallel and antiparallel magnetic configurations, *Physical Review B* **105**, 064427 (2022).
- [53] J. Barker and G. E. W. Bauer, Thermal spin dynamics of yttrium iron garnet, *Phys. Rev. Lett.* **117**, 217201 (2016).
- [54] L.-S. Xie, G.-X. Jin, L. He, G. E. W. Bauer, J. Barker, and K. Xia, First-principles study of exchange interactions of yttrium iron garnet, *Phys. Rev. B* **95**, 014423 (2017).